Enhanced light absorption in thin-film solar cells with light propagation direction conversion

Ikuo Suemune

Research Institute for Electronic Science, Hokkaido University, Kita-20, Nishi-10, Kita-ku, Sapporo 001-0020, Japan
*isuemune@es.hokudai.ac.jp

Abstract: Enhancement of optical absorption in thin-film solar cells (TF-SCs) has been the long-lasting issue to achieve high efficiencies. Grating couplers have been studied for the conversion of incident light into guided modes propagating along TF-SCs to extend optical path for higher optical absorption. However the wavelength band for the efficient conversion remained relatively narrow and the overall improvement of TF-SC efficiencies has been limited. This paper demonstrates that the grating height design as well as the phase matching condition is important for the enhancement of optical absorption in TF-SCs with the calculation of short-circuit currents as a figure of merit for optimization. The influence of the light absorption coefficients and grating coupling strengths on the light absorption bandwidth is also discussed.

OCIS codes: (050.1950) Diffraction gratings; (050.2770) Gratings; (300.1030) Absorption; (350.6050) Solar energy.

References and links

1. M. Konagai, "Present status and future prospects of silicon thin-film solar cells," Jpn. J. Appl. Phys. **50**, 030001 (2011).
2. Y. Tsunomura, Y. Yoshimine, M. Taguchi, T. Baba, T. Kinoshita, H. Kanno, H. Sakata, E. Maruyama, and M. Tanaka, "Twenty-two percent efficiency HIT solar cell," Sol. Energy Mater. Sol. Cells **93**(6-7), 670–673 (2009).
3. M. A. Green, K. Emery, Y. Hishikawa, and W. Warta, "Solar cell efficiency tables (version 37)," Prog. Photovolt. Res. Appl. **19**(1), 84–92 (2011).
4. E. Yablonovitch and G. D. Cody, "Intensity enhancement in textured optical sheets for solar cells," IEEE Trans. Electron. Dev. **29**(2), 300–305 (1982).
5. J. Nelson, *The Physics of Solar Cells* (Imperial College, 2003).
6. M. Kroll, S. Fahr, C. Helgert, C. Rockstuhl, F. Lederer, and T. Pertsch, "Employing dielectric diffractive structures in solar cells – a numerical study," Phys. Status Solidi., A Appl. Mater. Sci. **205**(12), 2777–2795 (2008).
7. J. Zhu, Z. Yu, G. F. Burkhard, C.-M. Hsu, S. T. Connor, Y. Xu, Q. Wang, M. McGehee, S. Fan, and Y. Cui, "Optical Absorption Enhancement in Amorphous Silicon Nanowire and Nanocone Arrays," Nano Lett. **9**(1), 279–282 (2009).
8. Y. Lu and A. Lal, "High-efficiency ordered silicon nano-conical-frustum array solar cells by self-powered parallel electron lithography," Nano Lett. **10**(11), 4651–4656 (2010).
9. Q. Chen, G. Hubbard, P. A. Shields, C. Liu, D. W. E. Allsopp, W. N. Wang, and S. Abbott, "Broadband moth-eye antireflection coatings fabricated by low-cost nanoimprinting," Appl. Phys. Lett. **94**(26), 263118 (2009).
10. J. K. Hyun, C. Ahn, H. Kang, H. J. Kim, J. Park, K.-H. Kim, C. W. Ahn, B. J. Kim, and S. Jeon, "Soft elastomeric nanopillar stamps for enhancing absorption in organic thin-film solar cells," Small **9**(3), 369–374 (2013).
11. K. R. Catchpole, "A conceptual model of the diffuse transmittance of lamellar diffraction gratings on solar cells," J. Appl. Phys. **102**(1), 013102 (2007).
12. C. Eisele, C. E. Nebel, and M. Stutzmann, "Periodic light coupler gratings in amorphous thin film solar cells," J. Appl. Phys. **89**(12), 7722–7726 (2001).
13. N. Senoussaoui, M. Krause, J. Mueller, E. Bunte, T. Brammer, and H. Stiebig, "Thin-film solar cells with periodic grating coupler," Thin Solid Films **451–452**, 397–401 (2004).
14. H. Stiebig, N. Senoussaoui, C. Zahren, C. Haase, and J. Muller, "Silicon thin-film solar cells with rectangular-shaped grating couplers," Prog. Photovolt. Res. Appl. **14**(1), 13–24 (2006).
15. C. Haase and H. Stiebig, "Optical properties of thin-film silicon solar cells with grating couplers," Prog. Photovolt. Res. Appl. **14**(7), 629–641 (2006).
16. S. Na, S.-S. Kim, S.-S. Kwon, J. Jo, J. Kim, T. Lee, and D.-Y. Kim, "Surface relief gratings on poly(3-hexylthiophene) and fullerence blends for efficient organic solar cells," Appl. Phys. Lett. **91**(17), 173509 (2007).

#182785 - $15.00 USD Received 9 Jan 2013; revised 12 Apr 2013; accepted 19 Apr 2013; published 25 Apr 2013

17. I. Tobías, A. Luque, and A. Marti, "Light intensity enhancement by diffracting structures in solar cells," J. Appl. Phys. **104**(3), 034502 (2008).
18. L. Zeng, Y. Yi, C. Hong, J. Liu, N. Feng, X. Duan, L. C. Kimerling, and B. A. Alamariu, "Efficiency enhancement in Si solar cells by textured photonic crystal back reflector," Appl. Phys. Lett. **89**(11), 111111 (2006).
19. R. Dewan and D. Knipp, "Light trapping in thin-film silicon solar cells with integrated diffraction grating," J. Appl. Phys. **106**(7), 074901 (2009).
20. D. Madzharov, R. Dewan, and D. Knipp, "Influence of front and back grating on light trapping in microcrystalline thin-film silicon solar cells," Opt. Express **19**(S2 Suppl 2), A95–A107 (2011).
21. S. H. Lim, D. Derkacs, and E. T. Yu, "Light scattering into silicon-on-insulator waveguide modes by random and periodic gold nanodot arrays," J. Appl. Phys. **105**(7), 073101 (2009).
22. A. Moreau, R. Smaali, E. Centeno, and C. Seassal, "Optically optimal wavelength-scale patterned ITO/ZnO composite coatings for thin film solar cells," J. Appl. Phys. **111**(8), 083102 (2012).
23. I. Suemune, "Conversion of light propagation direction for highly efficient solar cells," Appl. Phys. Express **4**(10), 102301 (2011).
24. K. Yee, "Numerical solution of initial boundary value problems involving maxwell's equations in isotropic media," IEEE Trans. Antenn. Propag. **14**(3), 302–307 (1966).
25. A. Taflove, "Application of the finite-difference time-domain method to sinusoidal steady-state electromagnetic-penetration problems," IEEE Trans. Electromagn. Compat. **EMC-22**(3), 191–202 (1980).
26. I. Tobías, A. Luque, and A. Marti, "Light intensity enhancement by diffracting structures in solar cells," J. Appl. Phys. **104**(3), 034502 (2008).
27. J. G. Mutitu, S. Shi, C. Chen, T. Creazzo, A. Barnett, C. Honsberg, and D. W. Prather, "Thin film solar cell design based on photonic crystal and diffractive grating structures," Opt. Express **16**(19), 15238–15248 (2008).
28. P. Wuerfel, *Physics of Solar Cells* (Wiley-VCH, 2009).
29. L. Ley, *The Physics of Hydrogenated Amorphous Silicon, Springer Tracts Appl. Phys.* Eds. J.D. Joannopoulos, G. Lucovsky (Springer, 1984) **56,** Chap. 3.
30. X. Jing and Y. Jin, "Transmittance analysis of diffraction phase grating," Appl. Opt. **50**(9), C11–C18 (2011).

1. Introduction

Among presently available photovoltaic (PV) technologies, crystalline-silicon (Si) solar panels are dominating the market [1–3]. From the viewpoint of saving Si material resources and the cost reduction, thin-film solar cells (TF-SCs) have been expected to play a major role. However TF-SCs generally face the problem of reduced optical absorption efficiency especially in the long-wavelength band where optical absorption coefficient is diminishing toward the longer wavelength. There have been several proposals to improve the optical absorption efficiencies of TF-SCs. One of the most commonly adopted method is a textured structure [4] where incident light scattered at textured surfaces and interfaces propagates longer path lengths in thin-film optical absorption layers with total internal reflections. This method is practical and easy to incorporate into TF-SCs by employing for example inhomogeneously deposited transparent conductive oxide (TCO) surfaces. About 50-times absorption enhancement is predicted and best results around 10 times have been reported [5]. More intentional and deterministic structures such as incorporating diffraction gratings into TF-SCs have been extensively studied to manage photons to realize high-efficiency TF-SCs. Key issues for the photon management in TF-SCs are divided into two categories. One is antireflection of light incident on TF-SCs, and the other is trapping of incident light in TF-SCs [6].

Antireflection of incident light has been demonstrated for example with nanowires and nano-cone array structures [7,8]. These as well as the sub-wavelength-scale moth-eye structures [9,10] operate as very efficient antireflection surface structures. However this is the necessary but not sufficient condition to increase the TF-SC efficiencies. If the absorption within TF-SCs is low by the decrease of the absorption coefficient or by too thin absorption layer thickness, incident light will be reflected back again from back metal electrodes. Incident light transmitted through these surface structures needs to be efficiently trapped and absorbed in TF-SCs.

Trapping of incident light has been actively studied employing diffraction gratings. One of the main ideas is to suppress zeroth-order diffraction and to diffract incident light into higher-order diffraction modes so that the diffraction angles are beyond the light escape cone [11–17]. However in the case of thin absorption layers, diffracted light is reflected back to the gratings from the counter interfaces and additional diffraction at the gratings results in optical

#182785 - $15.00 USD Received 9 Jan 2013; revised 12 Apr 2013; accepted 19 Apr 2013; published 25 Apr 2013

loss by the outward light scattering. To prevent this kind of secondary diffraction loss, additional structures have been invented. One of them is to combine the gratings with back reflectors, such as distributed Bragg reflectors (DBRs) [18] or back metal electrodes [19]. The other is to include another grating with a different height at the counter interface so that the diffracted light propagation is controlled into different diffraction orders and then the secondary diffraction loss is prevented [20].

The other idea for trapping incident light is the application of grating couplers to TF-SCs. This is to convert incident light into guided modes propagating along a light absorption layer in a TF-SC and to extend the optical path for efficient optical absorption [6,21]. However generations of guided modes are generally limited to narrow spectral bands [6,22] and the contribution of this scheme to the overall improvement of TF-SC efficiencies has been limited so far. We have proposed a design concept of the grating height so that the phase shift of an incident light wave front passing through the grating to be π and demonstrated efficient and wide-band optical absorption enhancement [23]. However since the function of grating couplers can cover a part of the solar cell wide spectral range, the impact of this new design on the solar cell performance needs further examinations. In this paper, we examine the π-phase shift concept with the calculation of short-circuit currents as a figure of merit for optimizing TF-SC. The influence of optical absorption coefficients and grating coupling strengths on the optical absorption bandwidth is also discussed.

2. Calculation of short-circuit current for a silicon thin-film solar cell

A silicon TF-SC dealt with in this paper is schematically shown in Fig. 1(a). On a SiO_2 substrate an indium tin oxide (ITO) electrode with the thickness of H_{ITO} and a silver (Ag) electrode sandwich the light absorbing amorphous-silicon (a-Si) layer with the thickness of H_{Si}. At the interface of the ITO electrode and the a-Si layer a grating with the height of H_{grat} composed of ITO and a-Si regions is inserted where each part has the same length of half the period D. In this structure the grating cannot be treated as a perturbation and the electromagnetic-field propagation was calculated with the finite-difference time-domain (FDTD) numerical simulations [24,25]. The FDTD simulation is a computational electrodynamic modeling technique to calculate the Maxwell's differential equations directly by replacing the partial differential terms with finite difference equations and is known to give accurate results with a small enough grid size. In the present simulation the grid size of 1/60 of λ/n_{Si} was employed, which is 3.2 nm for the wavelength of λ = 800 nm and is small enough for high accuracy. The FDTD simulations were performed with two-dimensional modeling. A plane-wave down-propagating light source was set above the TF-SC and simulations were started upon light incidence with step-function time dependence until the electromagnetic fields approached steady states with low enough time-fluctuations. The reflection and transmission (in case of transparent substrates) were evaluated with power monitors set above the light source and below the TF-SC, respectively, by calculating the time-averaged power flow, i.e., the Poynting power,

$$\boldsymbol{P} = \oint_S \boldsymbol{E} \times \boldsymbol{H} \cdot \boldsymbol{n} dS, \tag{1}$$

#182785 - $15.00 USD Received 9 Jan 2013; revised 12 Apr 2013; accepted 19 Apr 2013; published 25 Apr 2013

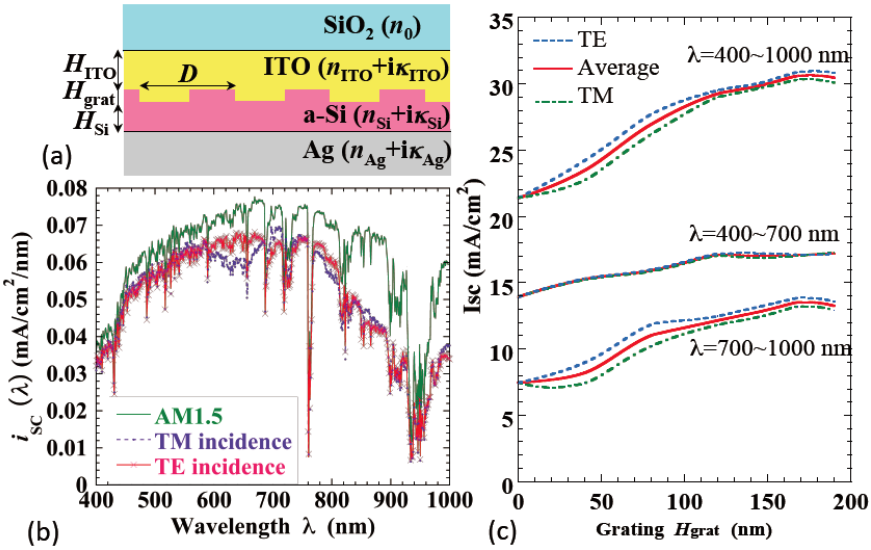

Fig. 1. (a) Schematic of the calculated silicon TF-SC. (b) Wavelength dependence of short-circuit current under AM1.5 spectral irradiance. Solid line under 100%absorption efficiency, dashed line for TM incidence, and solid line with × for TE incidence. (c) Spectrally integrated short-circuit current vs. grating height H_{grat}.

where $\boldsymbol{n}$ is the unit vector normal to the monitor surface S. Optical absorption was calculated by setting monitors covering respective optical absorption regions. Accuracy of the simulations was examined by setting another monitor covering the whole area, which monitors the whole radiation power and optical absorption, and these values were compared with the sum of the above monitors. The agreement of the two methods was within the error less than 0.5% in most cases.

We assume an electromagnetic plane wave incident from the upper SiO_2 region with the refractive index of n_0. For simplicity we do not consider additional interfaces above the SiO_2 region. In conventional grating couplers a normal incident wave is coupled to guided modes propagating along a waveguide, which is the a-Si layer in the present structure, when the phase matching condition,

$$D = m_D \lambda / N_{eff}, \tag{2}$$

is satisfied, where N_{eff} is the effective refractive index of a guided mode and m_D is an integer. Gratings are generally regarded as "perturbation" to the guided mode and the coupled guided mode propagates many grating periods laterally. This results in the wavelength selectivity for efficient mode conversion and sharp absorption peaks are generally observed [6,21,22]. This is the excellent feature for grating coupler applications to excite guided modes with monochromatic incident light. However this wavelength selectivity prevents wideband optical absorption for SC applications.

We have proposed to set the phase shift of an incident-light wave front passing through a grating to be π for efficient and wide-band optical absorption enhancement [23]. This sets the condition on the grating height H_{grat} in Fig. 1(a) as

$$\frac{2\pi |n_{Si} - n_{ITO}| H_{grat}}{\lambda} = \pi, \tag{3}$$

where the imaginary parts of the complex refractive indices, $n_{Si} + i\kappa_{Si}$ and $n_{ITO} + i\kappa_{ITO}$ for a-Si and ITO, respectively, were neglected to evaluate the phase shift. This condition modulates the light wave front periodically by the phase π at the exit plane of the grating region. This naturally

#182785 - $15.00 USD Received 9 Jan 2013; revised 12 Apr 2013; accepted 19 Apr 2013; published 25 Apr 2013

generates the "standing wave" in the a-Si layer underneath the grating. This together with the phase matching condition given in Eq. (2) efficiently converts the normal incident wave to the wave propagating along the a-Si optical absorption layer with much less grating periods than conventional grating couplers [23]. Here we examine this proposal with the calculation of short-circuit currents as a figure of merit to optimize the silicon TF-SC.

We calculate short-circuit currents under normal illumination. We assume that all the photons absorbed by the silicon layer are converted into electron-hole pairs and that the photo-generated carriers all contribute to short-circuit current and thus concentrate to the optical design of the TF-SC. Then the short-circuit current is given by the following equations [26,27],

$$I_{SC} = \int i_{SC}(\lambda) d\lambda \ [\mathrm{mA/cm^2}], \tag{4a}$$

$$i_{SC}(\lambda) = \frac{q}{hc} \lambda \cdot QE(\lambda) \cdot S(\lambda) \ [(\mathrm{mA/cm^2})/\mathrm{nm}], \tag{4b}$$

where q, h, and c are the electron charge, the Planck constant, and the light velocity in vacuum. $QE(\lambda)$ is the wavelength dependent absorption efficiency in the a-Si region calculated with the FDTD simulation. $S(\lambda)$ is the wavelength dependent air mass (AM)1.5 spectral irradiance in the unit of [mW/cm^2/nm] [28].

Figure 1(b) is the calculated wavelength dependence of the short-circuit current, $i_{SC}(\lambda)$. The refractive indices used for the calculations are $n_0 = 1.45$ for the SiO_2 substrate and $n_{ITO} + i\kappa_{ITO} = 1.85 + i0.01$for ITO. Dispersive complex refractive indices were employed for the a-Si layer and the Ag electrode from the RSoft Material Library and the typical values at the wavelength of 800 nm are $n_{Si} + i\kappa_{Si} = 4.23 + i0.104$ and $n_{Ag} + i\kappa_{Ag} = 0.173 + i5.02$, respectively. The data used for a-Si is for the one without hydrogenation and shows longer absorption tail toward the longer wavelength [29]. Optical absorption coefficients generally decrease for the longer wavelength, and we tentatively set the center wavelength as 800 nm for the evaluation of Eqs. (2) and (3). For the structure shown in Fig. 1(a), Eq. (3) determines the optimum grating height as $H_{grat} = 168$ nm. For the demonstration of the high efficiency of the present design, a thin a-Si layer of $H_{Si} = 50$ nm was assumed. The period of the grating D depends on N_{eff} in Eq. (2), which is dependent on either transverse electric (TE) or transverse magnetic (TM) polarization of the incident light. Also the increase of the grating portion modifies the guided mode properties and therefore N_{eff}. Based on these situations, the grating period D was determined from the numerically calculated D dependences of the absorption efficiency (not shown), and D was given as 450 nm in Fig. 1. The solid (green) line is for the case of 100% absorption efficiency, the dashed (purple) line for the TM-polarized light incidence, and the solid (red) line with × for the TE-polarized light incidence.

Their spectral integrations from 400 nm to 1000 nm are given in Fig. 1(c) for different H_{grat}. Although the TE and TM polarizations of the incident light result in the different wavelength dependences of the absorption efficiency as shown in Fig. 1(b), the integrated short-circuit current I_{SC} shows the moderate difference. It gradually increases with the increase of H_{grat} (maximum value is 36.8 mA/cm^2). It is generally expected that optical absorptions increase with the increase of the absorption layer thickness (this applies for the a-Si grating height in the present case). However it is noted that the situation is not so simple as revealed in our previous investigations [23], and the increase of the a-Si layer thickness can reduce optical absorption due to the increase of optical reflection and/or transmission. Therefore the smooth increase of the short-circuit current shown in Fig. 1(c) is not a trivial result but is the effect of the grating coupler. When the spectral integration of $i_{SC}(\lambda)$ is divided into the two regions of 400~700 nm and 700~1000 nm, the former shows more moderate H_{grat} dependence with less polarization sensitivity. In this range the main factor is the reduction of the reflectivity and the grating works as an antireflection coating that diffuses incident light. In the latter wavelength range I_{SC}

#182785 - $15.00 USD Received 9 Jan 2013; revised 12 Apr 2013; accepted 19 Apr 2013; published 25 Apr 2013

increases by 1.8-times from 7.5 to 13.7 mA/cm^2 for the increase of the grating height up to ~170 nm and saturates (maximum value is 17.7 mA/cm^2). In this wavelength range the grating functions as the propagation direction converter as is shown in the next section. This is the result consistent with the optimum grating height of H_{grat} = 168 nm predicted by the π-phase shift condition of Eq. (3).

3. Influence of absorption coefficients and grating coupling strength

In this section, we focus on the grating's function to convert the incident-light propagation from the normal direction to the one along the optical absorption layer. For this purpose we deal with a simpler structure shown in Fig. 2(a). It consists of an a-Si layer with the thickness of H_{Si} and the a-Si/air grating with the height of H_{grat} and the period D on a transparent SiO_2 substrate. The incident light was set to the TM polarization. The a-Si layer thickness H_{Si} was set to 100 nm and the grating period D was set to 330 nm with additional calculations on the D dependence at the wavelength of 800 nm (not shown). For the a-Si/air grating, Eq. (3) gives the optimum grating height as H_{grat} = 124 nm at the wavelength of 800 nm. Calculated spectra of the absorption efficiency are shown in Fig. 2(b) for three cases of H_{grat} = 0, 30, and 124 nm. The increase above the line for H_{grat} = 0 nm is the contribution of the grating. Similar to the discussion for Fig. 1(c), the enhancement in the wavelength region shorter than 700 nm is mainly due to the antireflection effect. The enhancement in the one longer than 700 nm shows the peaks around the wavelength of 800 nm mainly due to the phase matching condition of Eq. (2). As is seen in Fig. 2(b) the relevant spectra are not simple function of the grating height. This is because the grating coupler we are dealing with is in the strong coupling regime.

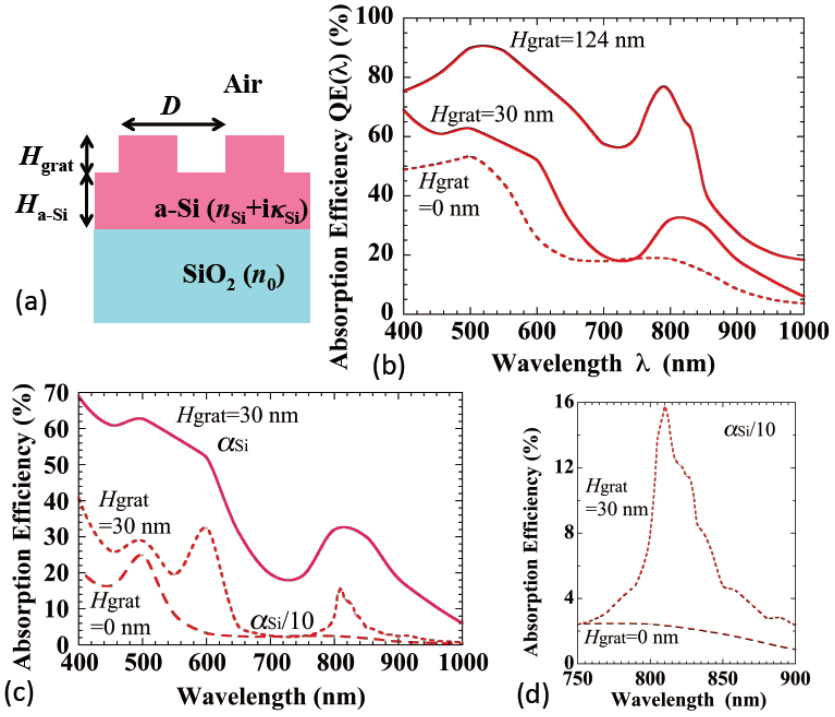

Fig. 2. (a) Schematic structure for the FDTD calculation. (b) Optical absorption efficiency calculated for the grating height of H_{grat} = 0, 30, and 124 nm. (c) Comparison of optical absorption efficiencies for H_{grat} = 30 nm with the a-Si absorption coefficient (solid line) and with virtual /10 (dashed line) where the one for H_{grat} = 0 nm with /10 is also shown as a reference. (d) Expanded spectrum around the 810-nm peak in (c).

#182785 - $15.00 USD Received 9 Jan 2013; revised 12 Apr 2013; accepted 19 Apr 2013; published 25 Apr 2013

For the purpose of clarifying the factors which determine the absorption peak width around 800 nm, the a-Si absorption coefficient, which is given by $\alpha_{Si} = 2\pi\kappa_{Si}/\lambda$, was virtually reduced to 1/10 for the FDTD calculations. This was applied to the cases of H_{grat} = 0 and 30 nm, and the calculated results are shown in Fig. 2(c) with the dashed lines. The peak around the wavelength of 800 nm was sharpened, and its spectral expansion is shown in Fig. 2(d). It is not a single peak but is composed of several peaks concentrated to this narrow spectral range.

To get more insight into these peaks, the field profiles calculated at the peak wavelength of 810 nm are shown in Fig. 3, where the transverse magnetic field H_y is shown for the TM-polarized incident light. Figure 3(a) is the field calculated with the given material refractive indices for the grating height of H_{grat} = 30 nm. The incident light beam was assumed to have the width corresponding to the 10 grating periods. The periodic field color change along the a-Si layer shows the formation of the standing wave and the lateral extension over several periods. When the a-Si absorption coefficient α_{Si} is virtually reduced to 1/10, the lateral propagation is much more extended as shown in Fig. 3(b). This is almost the same as the conventional grating coupler operation where incident light is efficiently converted to the guided modes along the (a-Si layer) waveguide. However this long distance propagation is possible by strictly satisfying the phase matching condition of Eq. (2), and this results in the narrow-band absorption enhancement. When the absorption coefficient α_{Si} is larger, the lateral field extension is limited by the optical absorption as shown in Fig. 3(a) and the light field is more confined to the excited grating region. This relaxes the phase matching condition and the bandwidth is more extended. The several peaks appeared in Fig. 2(d) is attributed to additional lateral spatial modulations of the standing wave, since the envelope of the standing waves in Fig. 3(b) is spatially modulated when the incident light wavelength is slightly detuned around 810 nm (not shown).

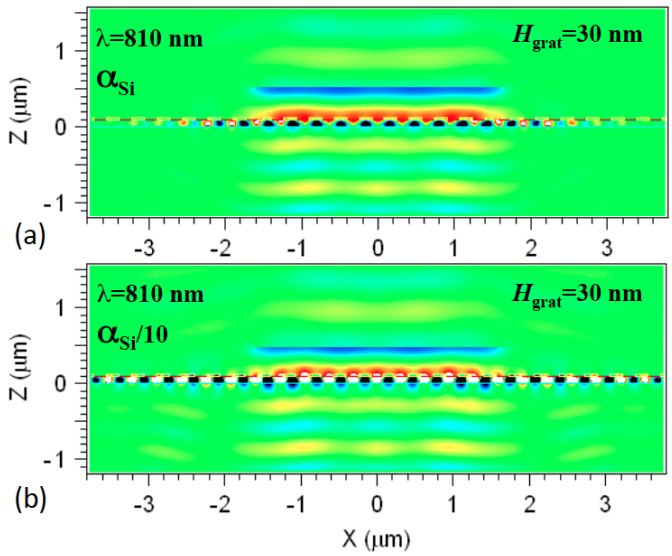

Fig. 3. (a) H_y field calculated with the a-Si absorption coefficient for the grating height of H_{grat} = 30 nm at the wavelength of 810 nm. The incident light beam was assumed to excite the width corresponding to the 10 grating periods. (b) Field calculated with virtually reduced absorption of /10.

#182785 - $15.00 USD Received 9 Jan 2013; revised 12 Apr 2013; accepted 19 Apr 2013; published 25 Apr 2013

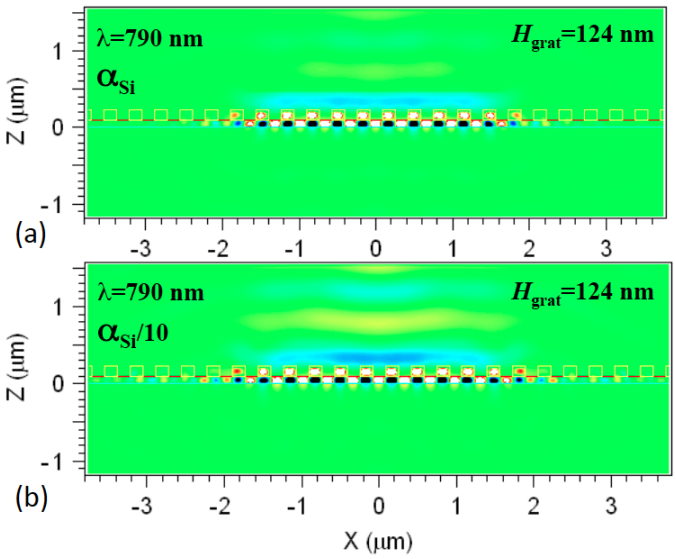

Fig. 4. (a) H_y field calculated with the a-Si absorption coefficient for the grating height of H_{grat} = 124 nm. (b) Field calculated with virtually reduced absorption of /10.

Similar study was performed for the grating height of H_{grat} = 124 nm. The H_y field calculated at the peak wavelength of 790 nm is shown in Fig. 4(a). The field is mostly confined to the excited area and penetrates laterally several periods in the similar manner as Fig. 3(a) for H_{grat} = 30 nm. The distinct difference appears when α_{Si} is virtually reduced to 1/10 as shown in Fig. 4(b). The field lateral extension seen in Fig. 3(b) does not take place and the field remained almost the same as Fig. 4(a). This demonstrates that the lateral field penetration is not limited by the a-Si layer optical absorption but the grating itself is limiting the field penetration along the a-Si layer. This takes place because of the strong coupling of the propagating light and the grating. Therefore this absorption peak width at around 790 nm for H_{grat} = 124 nm is determined by the coupling strength of the grating itself. It is noted that the absorption spectrum is almost insensitive to the change of the excitation beam width from 10 periods to 5 periods. This means that a few grating periods are enough to efficiently convert the incident-beam propagation direction toward the one along the a-Si absorption layer. In this regard the π-phase shift condition of Eq. (3) completely modifies the grating function from the conventional grating couplers to more strongly coupled light propagation direction conversion layer [23]. Then the remaining issue to study is the wavelength dependence of Eq. (3), that is, the deviation from the π-phase shift condition. For this purpose we replace π in the right-hand side with a general phase $\Phi(\lambda)$ in Eq. (3) and differentiate with λ. Then for the center wavelength of λ_0, the phase shift is derived approximately as

$$\Phi(\lambda = \lambda_0 + \Delta\lambda) \approx \pi(1 - \Delta\lambda / \lambda_0), \tag{5}$$

For the wavelength range of 700 to 900 nm covered by the grating coupler function in Fig. 2(b), the maximum deviation from the π-phase shift is 13%. This may not be negligible but the influence of this phase shift on the grating coupler function will be within limited range.

It is also noted that the comparison of the transmitted fields in Figs. 3 and 4 exhibits clear difference. The grating height in Fig. 3 does not satisfy the π-phase shift condition and substantial incident light is transmitted through the grating, while that in Fig. 4 does satisfy the condition and the transmitted light is almost suppressed. It is shown that the π-phase shift condition of the grating height for the present grating coupler is the same as the one for suppressing zeroth-order diffraction in diffraction gratings [30], and this explains the difference of the transmittance in Figs. 3 and 4. The main difference of our proposed grating coupler to the

#182785 - $15.00 USD Received 9 Jan 2013; revised 12 Apr 2013; accepted 19 Apr 2013; published 25 Apr 2013

diffraction gratings is that we do not enhance diffraction higher orders but focus to couple and convert incident light into guided waves (laterally propagating waves) along the waveguide (light absorption layer).

4. Discussion

In the above examples we applied the conditions of Eqs. (2) and (3) at the wavelength of 800 nm. This is the reason why the absorption peak appeared at around 800 nm in Fig. 2. The remaining issue is at what wavelength these conditions should be applied. In this regard, the combination of our proposed criteria and the numerical genetic optimization algorithms [6,22] will help to further optimize TF-SCs for any given dispersion of optical absorption coefficients.

7. Summary

We demonstrated that the grating height design to give the lateral π-phase shift is effective to enhance short-circuit current of the TF-SC. The absorption enhancement bandwidth broader than conventional grating couplers is due to the strong coupling of the grating to the laterally propagating light waves along the a-Si optical absorption layer. The present criteria will make the role of gratings more important for the improvement of TF-SCs.

Acknowledgments

The author wishes to thank K. Onodera of the Center for Innovation and Business Promotion, Hokkaido University, for his useful advice and suggestions.

#182785 - $15.00 USD Received 9 Jan 2013; revised 12 Apr 2013; accepted 19 Apr 2013; published 25 Apr 2013